Wave-induced collision loads and moments between a spar-buoy floating wind turbine and an installation vessel

Wave-induced collision loads and moments between a spar-buoy floating wind turbine and an installation vessel

D R Lande-Sudall[1], T S Høyven[1], K Herfjord[1] and T C Thuestad[1]

[1]Western Norway University of Applied Sciences, Inndalsveien 28, 5068 Bergen, Norway

E-mail: dla@hvl.no

Abstract. Spar-buoy floating wind turbines (FWTs) have been deployed at full-scale off the coast of Scotland. However, their deep draught restricts their wider-suitability for assembly and installation at shallow water ports. Here a barge-type installation vessel is investigated experimentally for supporting a FWT such that a draught reduction of up to 30% can be achieved. Tests in irregular waves are conducted to understand the design loads required of a mechanical linkage between the vessel and FWT. Overturning moments increase by over double for a doubling in significant wave height, H_s, and peak overturning moment occurs at the pitch eigenfrequency of the combined vessel and FWT. For H_s=1.5 m, these loads can be accommodated for with a steel truss-frame structure. Collisions between vessel and FWT are also tested for regular head waves and show that, whilst a number of collision forces exceed those of the relevant design standards, these could be reduced to within the existing design limits by use of a fender.

1. Introduction

Offshore wind is expected to be a one-trillion dollar global industry by 2040 [1], with a capacity exceeding 70 GW in Europe alone by 2030 [2]. To date, the majority of wind power plants are installed in shallow water locations with depths less than 40 m. To exploit the wind resource at deep water sites requires floating installations, and these are currently in development. Most recently, the world's first demonstration park, Hywind Scotland, featuring five, 6 MW floating wind turbines (FWTs) and utilising spar-buoy substructures, was installed off the coast of Peterhead, Scotland by Equinor. Assembly of these turbines, which feature a draught of over 70 m, was completed using the world's largest floating crane, Saipem 7000 at the deep water fjord outside, Stord, Norway. Few such deep water ports exist worldwide and so there is significant interest to make assembly of this floating technology more accessible. A number of novel installation methods have recently been proposed, with the aim of also reducing the number of weather-dependent offshore lifts, such as using a catamaran vessel supporting pre-assembled towers [3], or by horizontal tow-out and up-ending of the turbine at site [4]. In 2014, Equinor launched an innovation challenge, where several competing installation concepts for Hywind were presented. Amongst the three winners was a reusable transport frame proposed by Atkins [5], designed for both assembly and installation of spar-buoy FWTs. This installation method is the focus of the current work. The vessel features a mechanical turbine-vessel linkage which allows the FWT draught to be reduced for assembly and tow-out in shallower water. The FWT

can then be ballasted to the operational draft once at the wind farm site. The linkage is thus required to withstand overturning moments and possible collision loads induced by met-ocean conditions during tow-out and installation at site. The experimental work presented, evaluates the magnitude and occurrence of overturning moments between the connected vessel and FWT and possible impulse loads expected to occur when the FWT is separated from the vessel. A series of regular and irregular wave tests have been conducted on a 1:72 geometric scale model at the MarinLab towing tank, Western Norway University of Applied Sciences, Norway. Tests are presented for the full- and reduced-draught FWT for the following full-scale cases:

- connected FWT-vessel in irregular JONSWAP spectra with significant wave height, H_s varied between 1.5-3.5 m, and peak spectral period, T_P between 6.5-16.5 s;
- collision impulse between disconnected FWT and vessel under regular waves with H=1.5 and 2.9 m and T varied between 6.5-16.5 s.

Section 2 details the experimental model set-up and facility used for testing. Measurements of the moments of force between the connected FWT and vessel are presented in Section 3, with collision loads in Section 4. Conclusions and points of further work are addressed in Section 5.

2. Experimental method

The MarinLab towing tank is a 50 m long, 3.0×2.2 m section, test facility equipped with a six-flap Edinburgh Designs wavemaker and a four camera Qualysis motion-capture system with sampling frequency of 150 Hz. To simplify testing, a barge-type vessel, as opposed to the semi-submersible presented by Atkins [5], was built with dimensions detailed in Høyven [6] and summarised in Table 1. A diagram of the experimental set-up is shown in Figure 1. The barge was scaled such as not to exceed a maximum beam width of 0.6 m, in order to minimise the influence of blockage and reflections with tank walls. The FWT is Froude-scaled from the full-scale Hywind turbine dimensions from [7], with model geometry simplified from the original 'flask' form at the waterline, to a constant cylinder diameter of $D = 0.2$ m. Correct scaling of ballast and rotational inertia are ensured via modelling in DNV-GL Sesam. Due to material limitations, the draught of the model FWT could only be reduced by 18%, as opposed to an expected 30% at full-scale [6]. Both vessels were lightly moored to the tank walls, with four lines on the barge and two lines on the FWT. Each line had two springs connected in serial, providing a combined stiffness of approximately 6.6 N/m per line. A load cell rig, consisting of two tension/compression load cells (one Applied Measurements DDEN 250 N and one HBM U9C 500 N capacity), was fitted to the barge, allowing horizontal collision loads and overturning moments about the deck to be resolved. Two, 2000 N capacity, 12V RS Pro EM80 electromagnets attached to the load cell rig were used to automate release of the FWT from the barge in synchronisation with the wave phase.

Resistance-type wave gauges are used to measure the wave elevation at the model (digital signal) and also at 10 m in front of the model (both an analogue and digital signal were used here for synchronisation), to capture the undisturbed wave signal. Reflections from the model are noted to be very small at this upstream distance. The digital wave gauge signals are recorded at 128 Hz, whilst all analogue wave and force data are recorded through a National Instruments compact data acquisition system at 2000 Hz. For spectral analysis, all data are down-sampled to 128 Hz in post-processing. Collision analysis is conducted using the full 2000 Hz signal.

2.1. Load cell calibration

A load cell rig is used to mount the load cells to the barge and minimise off-axis loading, where load capacity is typically reduced to 50% of the rated capacity. To calibrate the rig, the load cells are firstly calibrated separately in both compression and tension directions, with five applied loads of between 0-200 N. The load cells are then assembled onto the rig, where a

Table 1: Main dimensions and particulars of the barge and FWT in full and model scales. Values in brackets ( ) indicate reduced-draught dimensions. Note the displacement mass of the FWT includes the tower top head mass.

Particular, unit	Notation	Barge		FWT	
		full	model	full	model
Overall length, m	L_{PP}	100	1.389	-	-
Beam, m	L_B	37	0.514	-	-
Diameter, m	D	-	-	14.4	0.2
Draught, m	T_B, T_F	4	0.056	76	1.06 (0.86)
Displacement mass, kg	m_B, m_F	1.30×10^7	33.85	1.15×10^7	30.06
Top head mass, kg	m_{th}	-	-	3.6×10^5	0.94
Centre of gravity above keel, m	KG_B, KG_F	3.77	0.052	26.42	0.367 (0.507)

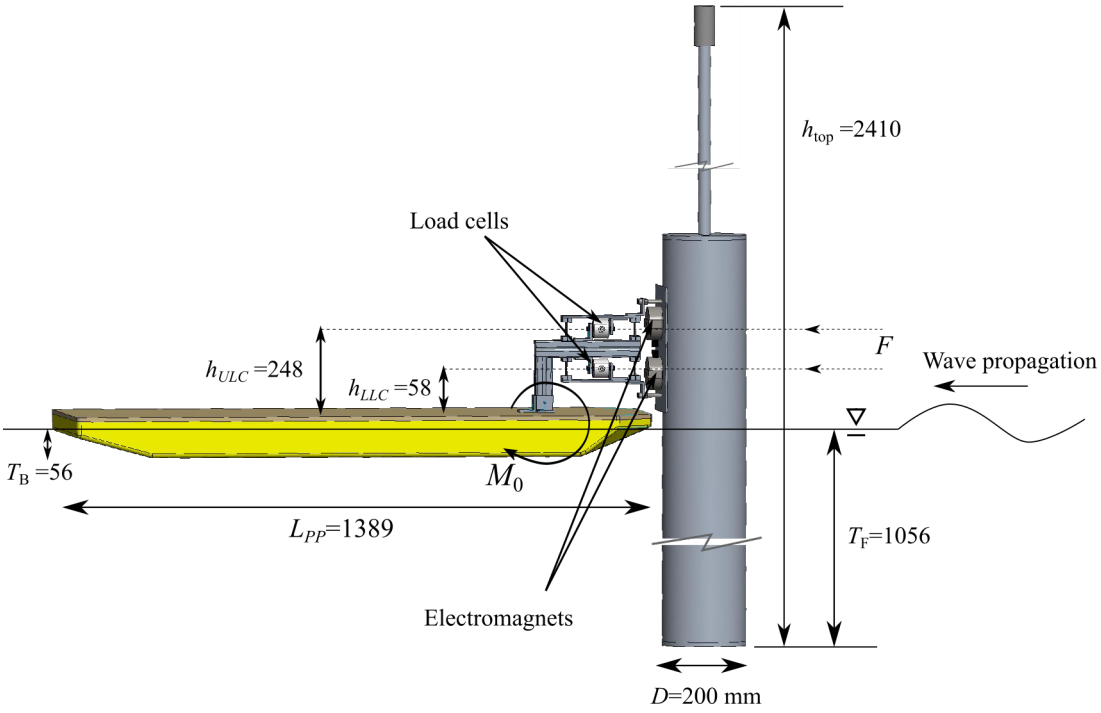

Figure 1: Side-view of connected barge and floating turbine model, showing direction of wave propagation, location of upper (ULC) and lower (LLC) load cells and electromagnets, and overall dimensions in millimetres.

second calibration is carried out at seven distances across the loading plate in both compression and tension directions, see Figure 2(a). The rig is shown to behave very linearly, Figure 2(b), with the difference between maximum measured and applied load not more than 5% at the edge of the loading plate. The discontinuity in the curves is due to the difference in vertical rig orientation when calibrating in tension and compression. A zero load offset is applied when mounted horizontally to the barge.

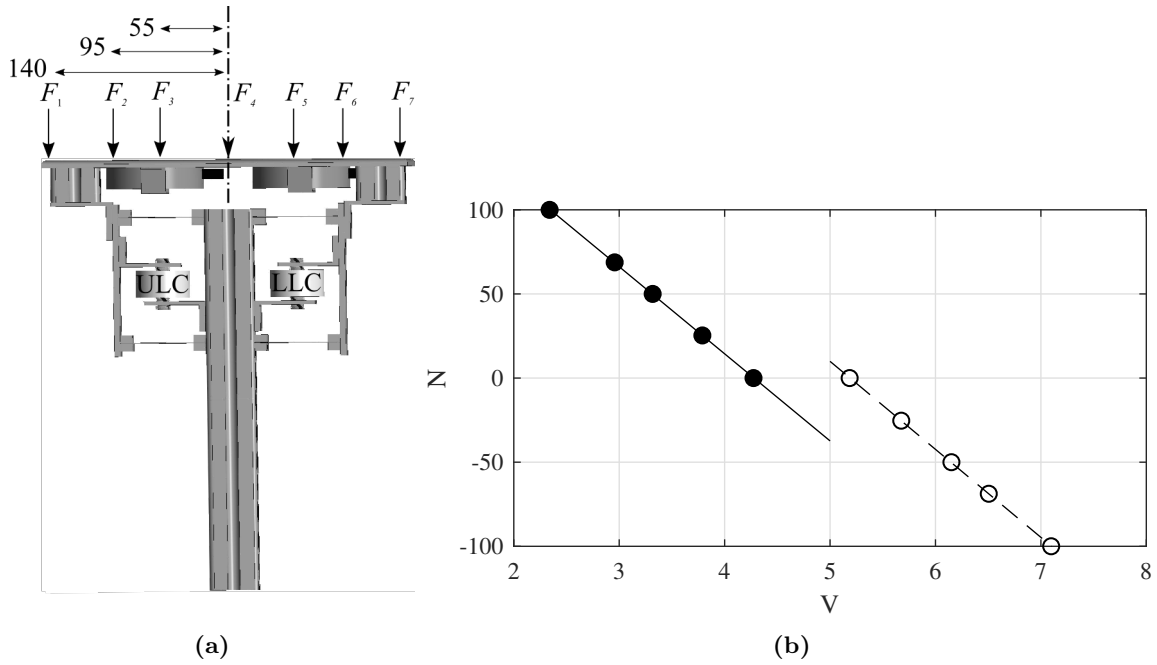

Figure 2: (a) Calibration of load cell rig, shown for compression, with seven load positions measured from the centreline and (b) a sample calibration curve of the upper load cell (ULC) for total calibration load varying between 0-200 N tension (—•) and compression (- - -○) applied at position F_4.

2.2. Wave calibration

All wave gauges are calibrated using a three-point calibration. Each set of wave spectra, S_{xx}, are measured for a 20-minute period without the model installed. A gain correction is then applied to ensure the wavemaker generates a measured spectral energy that is the same as the theoretical spectra across all wave frequencies, f. Due to time-constraints, gain-correction was not completed for spectra with $12.3 \leq T_P \leq 14.9$ s. Here, the same gain corrections from the closest available spectrum ($T_P = 10.5$ s or $T_P = 16.5$ s, respectively) were used to correct these spectra. This was found to give a very reasonable approximation to the requested spectra, as shown in Figure 3 when compared to the upstream wave gauge.

2.3. Decay testing

Prior to all testing, decay tests in heave, roll and pitch were conducted for the moored barge and FWT, both individually and connected (BFWT). The first eigenperiods for all decay tests are shown in Table 2. The reduced draught turbine was unstable alone, due to a negative metacentric height, and so no decay tests were conducted for this. A surge decay test for the connected BFWT was also conducted.

The decay time-series curves were least-squares fitted with an exponential sinusoidal decay curve, eq.(1):

$$y_n = A \sin\left(\sqrt{1-\zeta^2}\omega_0 t + \phi\right) e^{-\zeta\omega_0 t} \tag{1}$$

where A is the magnitude of the start of the oscillation curve, ζ the damping ratio, $\omega_0 = 2\pi f_0$ the un-damped natural frequency, and ϕ a phase shift. The heave response of the connected BFWT is highly damped, and so not accurate. Indeed, the heave eigenperiod corresponds to the frequency of the standing wave between the barge and tank walls triggered during the heave decay test. Instead, it was observed during irregular wave testing that the peak heave response

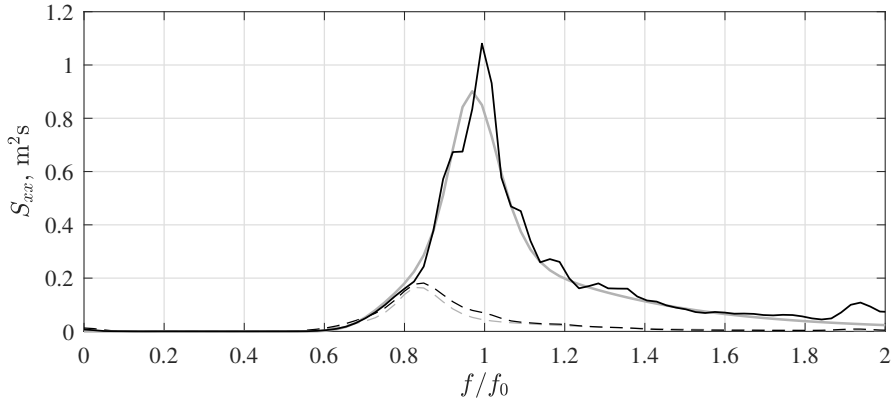

Figure 3: Comparison of measured, gain-corrected (black) and theoretical JONSWAP wave spectra (grey) for H_s=3.5 m and $T_P = 1/f_0$ s (—), H_s=1.5 m and T_P=16.5 s (- - -). Normalisation of the wave frequency, f is against the full-draught combined vessel and FWT pitch eigenfrequency, f_0 - see Section 2.3.

Table 2: Full-scale natural periods, $1/f_0$ (s), and damping ratio, ζ, for the lightly-moored barge, B, floating wind turbine (FWT) and combined vessel (BFWT) at full (FD) and reduced (RD) draught.

Mode	B		FWT_{FD}		BFWT_{FD}		BFWT_{RD}	
	s	[-]	s	[-]	s	[-]	s	[-]
Heave	8.5	0.02	18.5	0.02	8.5	0.03	8.6	0.03
Pitch	10.2	0.24	37.9	0.02	14.2	0.03	13.4	0.04
Roll	7.0	0.07	-	-	21.2	0.01	22.6	0.01
Surge	-	-	-	-	284.3	0.13	293.7	0.10

occurres at the same frequency as the pitch eigenfrequency, due to mode coupling. From here on, f_0 defines the pitch eigenfrequency of the BFWT at the corresponding draught of the test.

2.4. Test matrix

Loads between the connected FWT and barge were studied for a series of JONSWAP irregular wave-spectra, detailed in Table 3. Collision loads were investigated under regular long-crested waves, with full-scale wave height, H and period, T detailed in Table 4. For $H = 2.9$ m, wave periods greater than 12.3 s were not possible to test due to the load-carrying capacity of the electromagnets being exceeded, causing premature release of the FWT from the barge.

Table 3: Matrix of JONSWAP irregular wave parameters, H_s (m), and T_P (s), tested for the connected barge and FWT at full-draught (FD) and reduced draught (RD). Spreading parameter, γ, specified as 3.3 for all cases.

T_P / H_s	6.5		8.5		10.5		12.3		13.2		$1/f_0$		14.8		16.5	
	FD	RD	FD	RD	FD	RD	FD	RD	FD	RD	FD	RD	FD	RD	FD	RD
1.5	✓	✓	✓	✓	✓	✓	-	✓	✓	✓	✓	✓	✓	✓	✓	✓
3.5	✓	✓	✓	✓	✓	✓	-	✓	✓	-	✓	✓	✓	✓	✓	✓

Table 4: Matrix of regular sinusoidal wave height, H (m), and period, T (s), used for collision testing of barge and full-draught FWT, where f_0 is the full-draught combined BFWT pitch eigenfrequency. A minimum of five repetitions for each case were recorded.

H \ T	6.5	8.5	10.5	12.3	13.2	$1/f_0$	14.8	16.5
1.5	✓	✓	✓	✓	✓	✓	✓	✓
2.9	✓	✓	✓	✓	-	-	-	-

3. Moments between vessel and floating turbine

This section focuses on the loads occurring between the connected barge and FWT under irregular waves. Such loads may be expected during tow-out or assembly and thus give an indication of the design loads required of a mechanical linkage between the two.

3.1. Response of connected vessel

From the irregular sea-state test with $H_s = 1.5$ m and $T_P = 14.8$ s, the measured combined barge and floating wind turbine (BFWT) response amplitude operators (RAOs) in pitch and heave are shown in Figure 4(a) and are compared to a full-scale panel model in DNV-GL HydroD. Close agreement to the measured peak response is found at the respective pitch eigenfrequency. Deviations above and below this frequency are likely due to non-linear effects in the experiment and lack of accuracy in modelling of viscous forces. The peak response in pitch is greatest for the reduced draught BFWT, however, the corresponding peak from the moment-RAO in Figure 4(b), is less than the full-draught BFWT. This is presumably because despite net load being transmitted from a higher vertical position in the reduced draught case, the fully-ballasted vessel transmits greater net force. Here the moment-RAO is defined as the square-root of the moment-spectrum divided by the wave spectrum.

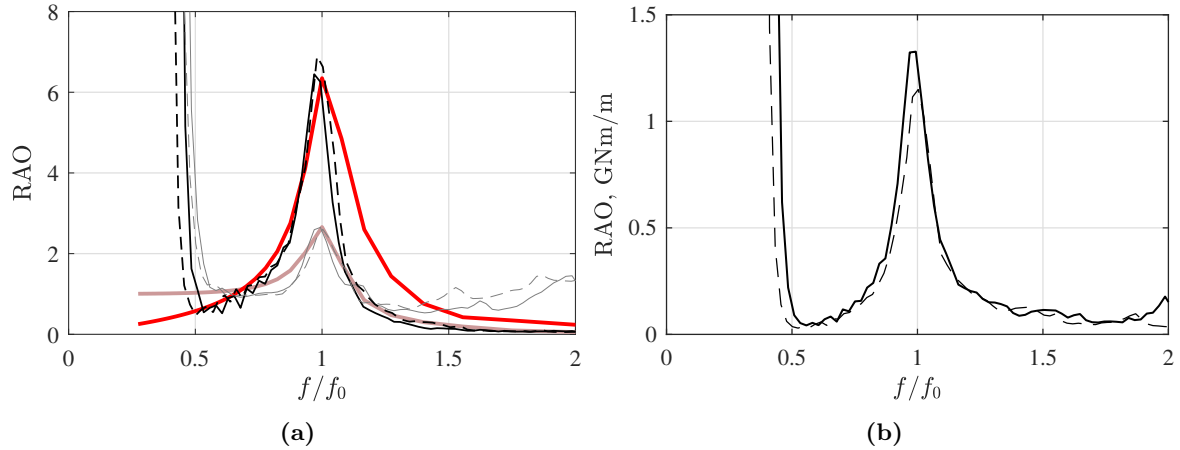

Figure 4: Response amplitude operators of the full (solid lines) and reduced (dashed lines) draught BFWT, for: (a) heave, m/m (faint colours) and pitch, deg/m (bold colours) response, compared with HydroD panel model (red thick lines in online version); and (b) moment response, GNm/m. All RAO's obtained as the square-root of the respective response spectrum divided by input wave spectrum for H_s=1.5 m and T_P=14.8 s.

3.2. Load occurrence statistics

The time-series history of overturning moment from each irregular sea-state test is discretised into 40 evenly-distributed bins of force-moment, Figure 5(a). The height of each bin indicates the probability density of occurrence for each moment interval. A normal distribution function is least-squares fit through the top-centres of each bin, providing the continuous probability density function. The normal distribution is found to give excellent agreement to each fully-developed sea-state, with only a small over-estimation ($< 10\%$) of the occurrence of loads at the extreme tails of the distribution, Figure 5(b).

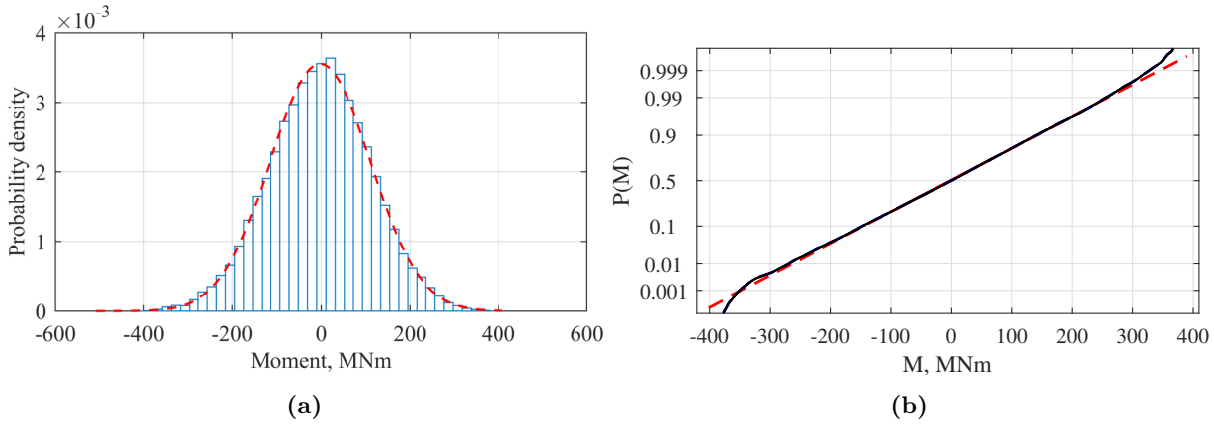

Figure 5: Probability density function (– – –) obtained by least-squares fitting of the binned-histogram (a) and corresponding normal probability plot against measured moment data (—) (b) for T_P=10.5 s, H_s=1.5 m.

In order to evaluate the distribution of extreme overturning moments between barge and turbine, the values of three standard-deviations (3σ), representing 99.7% probability interval of all load occurrences, is shown in Figure 6 for each sea-state, with full and reduced draught FWTs. Peak overturning moment coincides with the corresponding pitch eigenfrequency, f_0 of the combined barge and FWT, with an approximate doubling of load for a doubling in significant wave height. It is also seen that loads are consistently $\sim 10-20\%$ lower for the reduced draught case than full-draught. These results suggest that operations will be limited by the vessel's natural pitch frequency and operational wave height. In typical North Sea conditions [8], operationality would therefore be increased by a vessel with a greater pitch eigenperiod than the 13.7 s of the current full-scale barge.

These wave-induced overturning moments compare with an expected 4.24 GNm wind-induced overturning moment acting on the non-operating turbine, for a 10-metre mean wind-speed of 8 m/s (equivalent to a fully-developed sea-state with $H_s = 1.5$ m). This calculation is based on the method in [9], assuming a $1/7^{\text{th}}$ power-law shear profile to extrapolate wind-speed to hub-height [10] and a normal turbulence model with a reference turbulence intensity of 7.7% based on [11] for open-sea. Design loads are therefore dominated by wind-induced loads. Nevertheless, these loads could be supported by a square-based truss-frame structure accommodated on the barge deck. Following the method described in [12] for a simple Euler-Bernoulli beam, with an equivalent beam second moment of area representing the truss, I_{eq} eq.(2) given by [13], and using mild steel, the required footprint area is found to be 7 m^2. This assumes four legs of 2.5 m diameter forming the truss vertices, with cross-bracing forming the beam webbing.

$$I_{eq} = \frac{3}{2} A_c L^2 \tag{2}$$

A_c is the circular cross-section area in eq.(2) and L the centre-centre spacing of the truss legs.

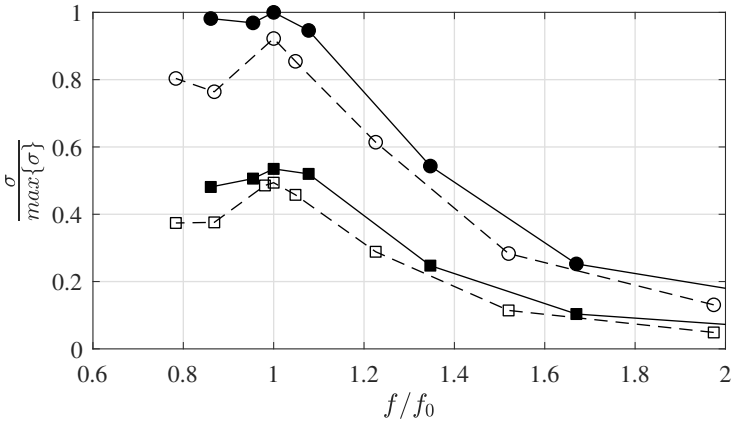

Figure 6: Comparison of 3σ normalised by maximum 3σ overturning moment versus normalised wave frequency, f/f_0 with H_s=1.5 m (□) and H_s=3.5 m (○), for the full draught (—, filled markers) and reduced draught (- - -, open markers) vessel. Here, $max\{3\sigma\} = 1.49$ GNm, full-scale.

4. Collision loads

A typical time-series of total measured force, wave elevation upstream of the device and release time for the electromagnets is shown in Figure 7(a). For all regular wave tests, consecutive collisions occurring with a period greater than the surge frequency of the barge (given in Table 2) are disregarded from the results, since these are likely a result of the light mooring system which would not be present at full-scale. This typically gave a minimum of four valid collisions occurring in each time-series, though for $H = 1.5$ m and $T < 10.5$ s, there were no collisions in some repeats. The impulse, I, of each collision is calculated as the area under the force-time curve, $F(t)$ (Figure 7(b)), between the start, t_i, and end, t_e, times of the collision according to eq. (3). Positive forces are defined in tension.

$$I = \int_{t_i}^{t_e} F(t)dt \tag{3}$$

In order to evaluate sensitivity of the release phase of the electromagnets relative to the wave phase, regular wave tests were conducted with $H = 2.9$ m, $T = 6.5$, 8.5 and 10.5 s, and the release phase of electromagnets varied in steps of $\pi/4$. This was shown in [6] to have no significant correlation to the magnitude of the collision impulse. For each of the remaining regular wave cases from Table 4, a minimum of five repetitions were conducted, such that the mean impulse could be calculated from typically 20 collisions for most cases.

Figure 8(a) shows that the maximum collision impulse coincides with the pitch eigenfrequency of the combined BFWT. The impulse for H=1.5 m is around 50% of that measured for H=2.9 m and so it is advantageous, indeed likely necessary, to operate in wave heights less than 3 m. Similarly, it is advantageous to operate in wave periods shorter than the natural period of the vessel. However, the impulse does not indicate the magnitude of peak load a mechanical linkage would be required to withstand. Figure 8(b) compares the impulse to the corresponding peak force from each collision with H=1.5 m. According to [14], the contact area between a service vessel and FWT is required to withstand 2.5 times the mass displacement of the vessel; in this case, 32.5 MN. From Figure 8(b), it is clear that a significant number of collisions exceed this design load. However, these tests have been for theoretically rigid and elastic collisions. For the

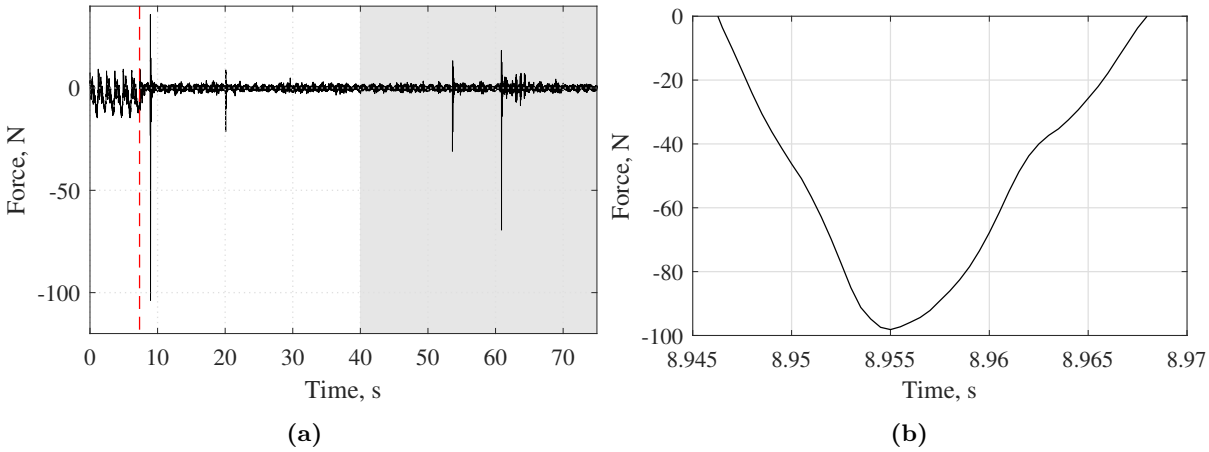

(a) (b)

Figure 7: (a) Model-scale force-time series (—) for $H = 1.5$ m, $T = 10.5$ s, showing magnet release point (- - -) and disregarded collisions (▬); (b) the area integrated under-the-curve for obtaining the impulse load, I, of the first collision from (a).

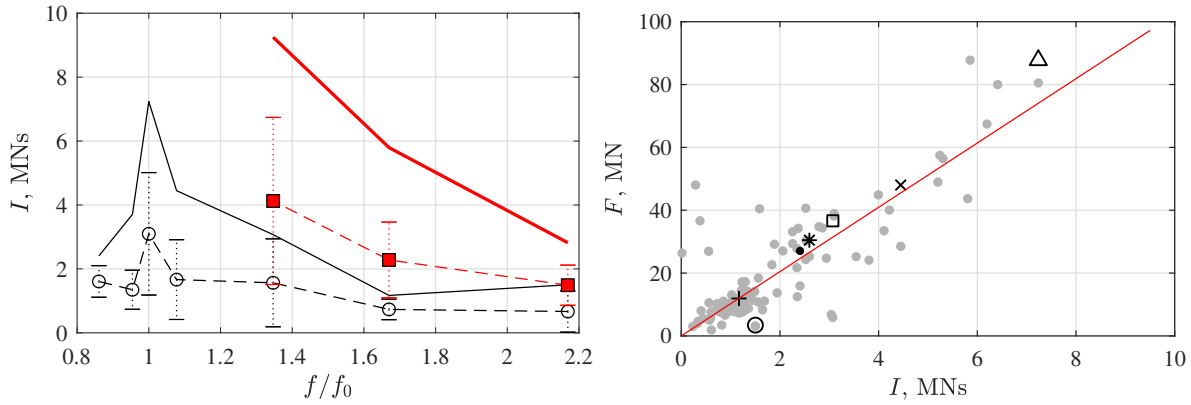

(a) (b)

Figure 8: (a) Variation in impulse loads, I, with normalised wave frequency, f/f_0 for wave height, H=1.5 m (mean: - - -○ and max: —) and H=2.9 m (mean: - - -■ and max: —). Error bars show $\pm\sigma$; (b) peak absolute collision force between the FWT and barge versus impulse, I, with least-squares linear-fit (—) to all collisions (•) and maximum collision forces from each regular wave set of H=1.5 m and T=6.5 (○), 8.5(+), 10.5(□), 13.2(×), 14.2 (Δ), 14.8 (*), 16.5 (●) s.

same impulse, the peak force could be reduced by around 50% by doubling the collision time, such as with a spring-damper system, i.e. a fender. This would bring the majority of collisions (over 95%) under the specified design load and therefore use of this installation method can be considered mechanically feasible.

5. Conclusions

Model tests on a barge-type installation vessel for floating spar-buoy wind turbines (FWTs) were conducted in order to investigate the feasibility of such an installation method. The barge allows the draught of the FWT to be reduced by up to 30% at full-scale and 18% model-scale. This

leads to a reduction in maximum overturning moment between the barge and FWT of around 10-20% compared to full-draught, across all wave peak periods tested. Such draught reduction is therefore beneficial not only for viability of shallower tow-out routes, but also for reducing loads on the mechanical linkage between vessel and FWT during tow-out. A truss-frame structure accommodated on the deck-space of the vessel could be designed to withstand these loads. Peak overturning moment occurred when the wave frequency aligned with the pitch eigenfrequency of the combined vessel and FWT. A vessel with lower eigenfrequency, such as a semi-submersible or frame, could be used to increase operationality in a wider range of sea-states. Collision loads in regular head seas was also investigated. Here, peak impulse occurred at the pitch eigenfrequency of the combined vessel and FWT. Use of a spring-damper fender could help reduce the maximum collision force, where a doubling of the collision time reduces the maximum collision force by around 50%. The experimental method employed in this work is general and applicable for other vessel types. Future work is focused on testing a new vessel, with lower pitch eigenfrequency and measuring loads in alternative wave headings. The acceleration of the top-head mass will also be investigated to assess limitations on loading of the turbine nacelle and components.

Acknowledgments
The authors would like to thank Gudmund Olsen and Equinor for support in building the model and for technical guidance.

References

[1] IEA 2019 World Energy Outlook - Executive Summary Tech. rep. International Energy Agency

[2] Nghiem A and Pineda I 2017 Wind energy in Europe: Scenarios for 2030 Tech. Rep. September WindEurope

[3] Jiang Z, Li L, Gao Z, Henning K and Christian P 2018 *Marine Structures* **61** 1–24 ISSN 0951-8339 URL `https://doi.org/10.1016/j.marstruc.2018.04.010`

[4] Hynne A 2010 *Numerisk og eksperimentell studie av transporten av Hywind med Windflip* Master's thesis NTNU

[5] Atkins 2017 Hywind floating wind Installation Challenge URL `https://www.atkinsglobal.com/en-GB/projects/hywind-installation-challenge`

[6] Høyven T S 2019 *Bending moments and collision loads between a floating offshore wind turbine and a supporting barge* Master's thesis University of Bergen

[7] Ulla T I 2014 Expanding into Deeper Waters: Development of the Hywind floating wind concept *BOEM-NREL Offshore Renewable Energy Workshop* (Sacramento: Statoil ASA) URL `https://www.boem.gov/NREL-Expanding-Deeper-Waters/`

[8] Mathiesen M, Meyer A K and Børge K 2014 Hywind Buchan Deep Metocean Design Basis RE2014-002 Tech. rep. Statoil

[9] Lande-Sudall D, Stallard T and Stansby P 2018 *Renewable Energy* **118** ISSN 18790682

[10] DNVGL 2014 *DNV-RP-C205 Environmental Conditions and Environmental Loads*

[11] Charnock H 1955 *Q.J.R. Meteorol. Soc.* **81** 639–640.

[12] Lande-Sudall D, Stallard T and Stansby P 2019 *Renewable and Sustainable Energy Reviews* **104** 492–503 ISSN 1364-0321 URL `https://doi.org/10.1016/j.rser.2019.01.035`

[13] Jalbi S and Bhattacharya S 2018 *Soil Dynamics and Earthquake Engineering* **113** 593–613 ISSN 0267-7261 URL `https://doi.org/10.1016/j.soildyn.2018.06.011`

[14] DNV-GL 2018 DNVGL-ST-0119 - Floating wind turbine structures Tech. Rep. July DNV-GL